THE JOURNAL OF PHYSICAL CHEMISTRY C

Article

Cite This: J. Phys. Chem. C 2019, 123, 2127−2138

pubs.acs.org/JPCC

Bay-Linked Perylenediimides are Two Molecules in One: Insights from Ultrafast Spectroscopy, Temperature Dependence, and Time-Dependent Density Functional Theory Calculations

Erik P. Farr, Matthew T. Fontana, Chen-Chen Zho, Peiqi Wu, Yolanda L. Li, Nicholas Knutson, Yves Rubin, and Benjamin J. Schwartz*

Department of Chemistry and Biochemistry, University of California, Los Angeles, Los Angeles, California 90095-1569, United States

Supporting Information

ABSTRACT: Bay-linked diperylenediimide (di-PDI) molecules are finding increasing use in organic electronics because of their steric hindrance that "twists" the two monomer units relative to one another, decreasing molecular aggregation. In this paper, we explore the electronic spectroscopy and ultrafast dynamics of the singly linked *β*-*β*-*S*-di-PDI (2,9′-di(undecan-5-yl)-2′,9-di(undecan-6-yl)-[5,5′-bianthra-[2,1,9-def:6,5,10-d′e′f′]diisoquinolin]-1,1′,3,3′,8,8′,10,10′(2*H*,2′*H*,9*H*,9′*H*)-octaone). Excitation−emission spectroscopy reveals two distinct emitting species, which are further characterized by time-dependent density functional theory (TD-DFT), demonstrating that the bay-linked PDI dimers exist in two geometrical conformations. These conformations are an "open" geometry, where the two monomer subunits are oriented nearly at right angles, giving them more J-like coupling, and a "closed" geometry, in which the two monomer subunits are nearly *π*-stacked, resulting in a more H-like coupling. Given the extent of through-space and through-bond coupling, however, neither di-PDI conformer can be well described simply in terms of independently coupled monomers; instead, a full quantum chemistry description is required to understand the electronic structure of this molecule. Temperature-dependent experiments and the TD-DFT calculations indicate that the "closed" conformer is ∼70 meV more stable than the "open" conformer, so that both conformers are important to the behavior of the molecule at room temperature and above. We use a combination of steady-state and femtosecond transient absorption and emission spectroscopies to globally fit the multiple electronic transitions underlying the spectra of both the "closed" and "open" conformers, which agree well with the TD-DFT calculations. The fact that di-PDI molecules are molecular species that adopt two distinct quasi-independent chemical identities has important ramifications for charge trapping and mobility in the organic electronic devices employing these materials.

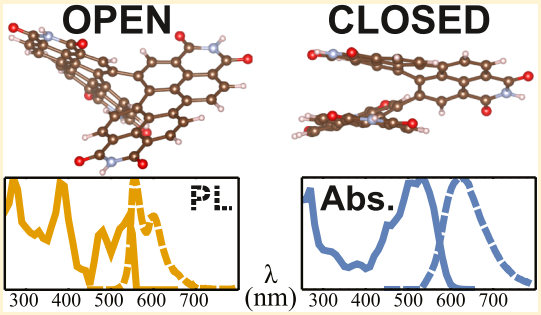

INTRODUCTION

Perylene and its derivatives are widely studied as model systems of molecular spectroscopy and aggregation, with work spanning many decades.[1−4] Recently, the organic electronics community has found numerous applications for perylenediimides (PDIs): not only are PDIs used in organic light-emitting diodes because of their generally high emission yields and high electrical conductivities[5,6] but they also serve as electron transport materials in organic photovoltaics (OPVs), with charge transport properties that can rival those of the more commonly used fullerenes.[1,7−12]

One advantage of PDIs for optoelectronic applications is that their structural and electronic properties can be independently synthetically controlled: substitutions to the electronically isolated N-termini can be used to tune solubility and aggregation without altering the base electronic properties, while substitutions on the *α* or *β* carbons (see Figure 1a) allow for control over the electronic properties of the delocalized *π* electrons.[13−15] PDIs and their derivatives have served as photostable pigments,[16] been central to studies of photo-induced charge transfer,[17,18] and helped to elucidate details of the physics of molecular aggregation.[9,16,19−22] For all of these reasons, considerable work has characterized the spectroscopy of PDIs as a function of both substitution[1,23,24] and degree of aggregation.[6,25]

Because of their large exposed *π* surface, PDIs are particularly prone to aggregation, allowing the chromophores on neighboring PDI molecules to interact.[3,4] The magnitude of the coupling between neighboring molecules depends strongly on their relative orientation. This is explained by the elegant theory developed by Kasha and co-workers,[26,27] which is outlined in Figure 1b: when the long axes of the two chromophores' transition dipoles are arranged in parallel, H-

Received: November 28, 2018
Published: December 27, 2018

DOI: 10.1021/acs.jpcc.8b11493
J. Phys. Chem. C 2019, 123, 2127−2138

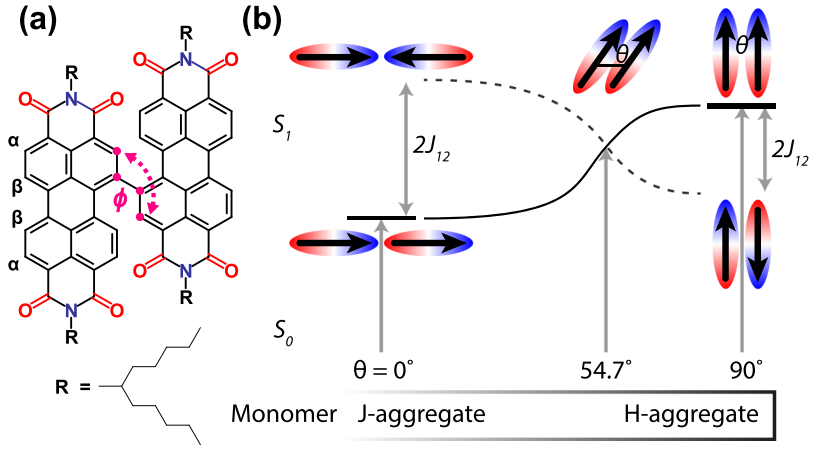

Figure 1. (a) General structure of β–β linked di-PDIs. For this (and previous[8]) studies, the −R groups consist of undecan-6-yl dovetails. (b) Qualitative schematic of ideal dipolar coupling (ideal J and H aggregation) between neighboring chromophores, showing the molecular geometries and energies of the excited electronic states whose transitions from the ground state are allowed (solid black) or forbidden (dashed). For the di-PDI whose structure is shown in (a), even though the chromophores are in close proximity because of the covalent bond between them, the subunits lie far from coplanarity and do not fit the ideal case. Thus, the magnitude of coupling between the PDI subunits is expected to be smaller than in a truly conjugated single molecule but larger than the case for typical intermolecular aggregation.

aggregate behavior (red-shifted emission with low quantum yield) results, whereas a head-to-tail configuration of the transition dipoles leads to J-aggregate behavior (blue-shifted emission with higher quantum yield).[19,28,29]

The simplest type of H- or J-aggregate behavior holds only for ideal molecular geometries and for crystal structures/dimers that have only one molecule per unit cell. However, outside of ideal conditions, both types of aggregation can emerge because of simultaneous coupling along multiple axes.[19,30] In addition, the presence of any charge-transfer interactions can also lead to coupling that is highly sensitive to sub-Å displacements between chromophores. This leads to the possibility of competing coupling factors that dictate whether or not the overall behavior resulting from aggregation is H-like or J-like. Thus, even though the Kasha picture successfully describes molecular coupling for a wide variety of molecular systems, additional considerations are required for systems that do not solely experience simple Coulombic coupling.[4]

The nature of molecular coupling in PDI systems has been well established through investigations on systems with precisely controlled coupling.[1] For example, several groups have prepared molecules with two PDI units held together cofacially at controlled distances by a molecular scaffold;[31,32] these PDI dimer constructs show attenuated and red-shifted photoluminescence spectra, which is reflective of the coupling between the monomer subunits.[31] These cofacially held PDI dimers have near-optimal π-stacking that also produces a lower-lying excimer state.[31]

This strong coupling between aggregated PDIs can be detrimental in certain applications, such as preventing charge separation in OPVs.[1] Thus, the use of PDI-based materials in organic solar cells requires some type of strategy to prevent aggregation. One simple strategy is to covalently link two PDIs together into dimers (di-PDIs), or several PDIs together into oligomers.[1,28] By covalently linking PDI units together, steric interactions between the individual molecules can disrupt intermolecular aggregation yet maintain excellent charge transport properties.[9,11,12] With dimers constructed using a single-bond linkage between PDI units at the β (also called bay)-position (see Figure 1a), conjugated polymer-based photovoltaics using di-PDIs as acceptors have shown highly competitive power conversion efficiencies of ∼10.6%.[1,11,12,33]

The increasingly widespread use of covalently linked PDIs in organic solar cells strongly suggests that it is worth revisiting their spectroscopy. It is important to note that in contrast to co-facial PDI dimers, which experience near-optimal π stacking, covalently linked di-PDIs are not cofacially oriented and also may be conjugated through the bay-linked bond. This means their behavior is quite different from that in previous studies for two important reasons. First, the intermolecular distance between chromophores (the ∼1.3−1.5 Å length of a C−C bond) is smaller than what is applicable for the Kasha theory and is appreciably less than the ∼4.5 Å interplane distances for cofacially oriented PDIs.[4,31] Second, there may be free rotation around the β–β linkage, opening the possibility that more than one low-energy conformation could be populated at room temperature. This adds complexity in that both the through-space and through-bond coupling between the monomer subunits could be angle dependent. Thus, despite the increasing popularity of di-PDI's for optoelectronic applications, it is not clear that there is a simple picture that explains their electronic structure and spectroscopy.

In this paper, we employ a suite of spectroscopic techniques, backed up by high-level quantum chemistry calculations, to investigate the fundamental electronic nature of di-PDIs. We choose to focus on a relatively simple di-PDI whose structure is given in Figure 1a. This particular molecule has branched alkyl groups at the N positions to confer solubility and otherwise has only a single degree of freedom between the PDI monomer units: rotation about the bay-linked bond, ϕ. We note that this particular di-PDI has previously been employed in organic solar cells, yielding an efficiency of ∼5%.[9] Through a series of steady-state and ultrafast time-resolved absorption and fluorescence measurements, we show that the spectroscopy of the di-PDI molecule considered here consists of contributions from two entirely separate chemical conformers. On the basis of the results of our time-dependent density functional theory (TD-DFT) calculations and the observed excited-state dynamics, we assign these two species to stable "open" (monomer subunits roughly at right angles) and "closed"

DOI: 10.1021/acs.jpcc.8b11493
J. Phys. Chem. C 2019, 123, 2127−2138

(monomer subunits twisted to π-stack together to the degree allowed by steric considerations) conformers at different local minima along the ϕ coordinate. We also show that although the spectral broadening and redshift of this di-PDI appear H-like, the coupling mechanism cannot be explained by the standard aggregation picture. Instead, our experiments and calculations indicate that the through-bond interactions do not allow a simple electronic treatment of this molecule as arising from two independently coupled monomers. All of our results have important implications for the use of di-PDI's in OPVs and other optoelectronic devices.

METHODS

All solvents were commercially purchased from Sigma-Aldrich and used as received. The di-PDI of Figure 1a and the corresponding PDI monomer were synthesized in-house following the procedures in ref 7. For the rest of this paper, except where otherwise specified, we use the term di-PDI to refer to the specific structure of Figure 1a, and the term mono-PDI to refer to the monomer of this molecule, with a H atom capping the structure where the bay linkage is severed.

Thin-film samples were prepared by spin-coating a 1% PDI or di-PDI solution (10 mg dissolved in 1 mL dichloromethane) onto a glass substrate at 4000 rpm for 10 s. The mono- and di-PDI film thicknesses were 80 and 55 nm, respectively. The cleaning procedure for the substrates consisted of sonicating the glass for 10 min each in a detergent solution, deionized water, acetone, and finally isopropyl alcohol.

Our cryogenic glassy-matrix PDI samples were prepared by dissolving di-PDI in 2-methyl tetrahydrofuran (THF) to a concentration of $\sim 1 \times 10^{-4}$ M. The di-PDI solution was then transferred to a Starna Cells 0.2 mm path length cuvette. This cuvette was then placed in a copper holder specifically designed for use with a cryostat. The cryostat was pumped under vacuum and cooled to liquid nitrogen temperature to form a glass. During glass formation, however, cavitation led to bubbles that altered the concentration of the di-PDI by possibly a few tens of percent. Thus, we report only relative yields and qualitative results for our cryogenic spectroscopy experiments.

Quantum chemistry calculations were performed using both the Gaussian16 package[34] and QChem 5.0.[35] Our DFT calculations were based on structures optimized using the PBE0 functional[36] with basis set 6-31++G* and Grimme's empirical D3 dispersion correction.[37] The dihedral angle ϕ of the di-PDI (the angle defined by $\alpha_1-\beta_1-\beta_2-\alpha_2$, labeled in magenta in Figure 1a) was fixed at a variety of angles from 30 to 140° and the rest of the molecule's geometry optimized at each ϕ to investigate how twisting of di-PDI changes its energetics and photophysics. We defined the zero of the dihedral using atoms from the shorter ends of the di-PDI molecule to minimize the effects of the constrained dihedral on puckering of the PDI subunits.[11,23,38−42] Solvent effects were simulated using a polarizable continuum model (PCM)[43] with a dielectric of 4.81 to represent chloroform. Our TD-DFT calculations were carried out with the same functionals described above and RPA correction. The Coulombic coupling between the chromophores in the two stable conformations of di-PDI was estimated by interaction of transition charges on each monomeric PDI subunit; the transition charges were obtained from Mulliken population analysis[44] of the transition density matrix of the monomer PDI's lowest excitation.

Steady-state absorption and fluorescence measurements were collected using a LAMBDA 25 UV−vis spectrometer and FluoroMax-3 (J-Y HORIBA) fluorimeter with 2.13×10^{-6} M di-PDI solutions, the concentration chosen to avoid self-absorption. Photoluminescence was collected at 22.5° with respect to the excitation beam, and the sample was positioned normal to the excitation axis. For all measurements, the slit widths (1 nm) and integration times (1.5 s) were held constant. Furthermore, all spectra reported in this paper were corrected for the known wavelength dependence of the detector and the monochromator response.

We note that many prior experiments exploring the nature of intermolecular coupling have exploited fixed crystalline axes between the chromophores, thereby allowing identification of Davydov splitting through polarization-sensitive spectroscopies.[3] For our di-PDI with its internal dihedral degree of freedom and amorphous solid structure, it is necessary to employ alternative techniques. Thus, we took advantage of femtosecond pump-probe spectroscopy in an attempt to independently characterize the distribution of dihedral angles and the nature of the underlying independent electronic transitions. Femtosecond transient absorption was probed in the wavelength range of 450−750 nm to a maximum of roughly 2.5 ns for both the mono-PDI and $\sim 1 \times 10^{-5}$ M di-PDI in solutions and thin films. The power dependence was studied, and for excitation densities <400 μJ cm^{-2}, the signals from the solution samples remained linear and the dynamics intensity-independent. In films, however, the measured spectral dynamics became nonlinear above 200 μJ cm^{-2} and therefore excitation densities were kept below this threshold. No concentration dependence to the solution signals was observed over the range yielding 0.2−0.6 OD at λ_{max}. Spectra were chirp-corrected and analyzed assuming a Gaussian instrument response of roughly 80−100 fs. Excitation wavelengths were selected to access either the lowest excited state (540−580 nm) or to promote the molecule directly to a higher-lying excited state (400 nm). Data were acquired using an Ultrafast Systems HELIOS spectrometer with 4 s of averaging per spectrum. More details of this laser system may be found elsewhere.[45]

We further characterized the excited-state dynamics of our chromophores by measuring their time-resolved fluorescence spectra using optical Kerr-gating spectroscopy. Briefly, the Kerr-gating measurement exploits the transient birefringence induced by a strong nonresonant femtosecond pulse in a "Kerr medium" situated between two orthogonal polarizers with a high extinction coefficient (ideally >1:10 000).[46] One short laser pulse is used to excite the fluorescent sample. The fluorescence is directed through the two polarizers and the Kerr medium. The second pulse is then applied to the Kerr medium after an appropriate optical delay. The polarization of the sample fluorescence is rotated only when spatiotemporally coincident with the transient birefringence in the Kerr medium: the action of the second pulse thereby allows a small fraction of the fluorescence through the second polarizer while the "Kerr gate" is open. We chose liquid CS_2 as our Kerr medium, and this choice, along with the collecting optics used in our detection scheme, afforded a time resolution of roughly 2 ps.

RESULTS AND DISCUSSION

The main goal of this paper is to investigate the effect of having a covalent linkage on the spectroscopy and conformation of di-

DOI: 10.1021/acs.jpcc.8b11493
J. Phys. Chem. C 2019, 123, 2127−2138

PDI. It is well known that the choice of the β–β linkage prevents PDI dimer–dimer aggregation, which is desirable for many applications. Di-PDI molecules, however, may occupy a variety of relative positions along the degree of freedom represented by rotation ϕ around the covalent linkage, and it is not immediately obvious which configurations, or how many, will be dominant. We expect the coupling between chromophores, both through space and through bond, to depend strongly on ϕ; thus, an important goal of this work is to understand the origin of the coupling mechanisms in di-PDIs and how they change with ϕ.

Di-PDI Spectroscopy Consists of Two Absorbing and Emitting Species. Figure 2 shows the solution and film absorption spectra of our chosen di-PDI molecule. The absorption is quite intense and takes place broadly across the visible, which is a hallmark feature for its selection in OPVs. The vibronic features and general spectral profile of the di-PDI absorption are far broader than those of the corresponding isolated monomer; see the Supporting Information. Others have phenomenologically labeled this broadening of the di-PDI spectrum as H-like due to the overall redshift and lower corresponding emission quantum yield compared to the monomer.[23,47] As discussed in conjunction with eq S1 of the Supporting Information, however, when we attempted to fit the di-PDI absorption profile based on the idea that its spectrum could be described as that of two weakly coupled monomer PDI monomers; we found that the fits were not robust.

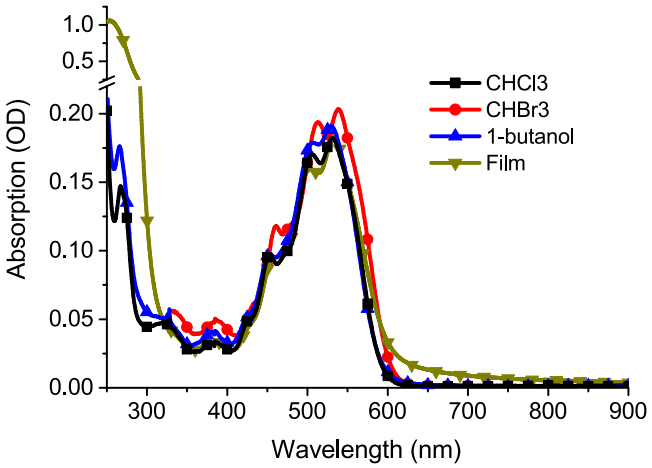

Figure 2. Steady-state absorption of purified 2.13×10^{-6} M di-PDI in chloroform (black squares), bromoform (red circles), 1-butanol (blue up-triangles), and as a 55 nm thick spin-cast film (dark yellow down triangles). The film absorption has been arbitrarily scaled for ease of comparison. Overall, the spectra are quite similar across solvents except for some fine differences in peak ratios, peak broadness, and some slight solvatochromic shifts. The maximum extinction coefficient in chloroform solution is roughly 70 000 M^{-1} cm^{-1} at 535 nm, and when integrated, the oscillator strength is nearly twice that of the monomer.

We also performed a series of fluorescence excitation–emission experiments on low-concentration (to avoid self-absorption and any potential aggregation) di-PDI solutions at room temperature, with the raw two-dimensional data shown in the Supporting Information. Figure 3 summarizes the results of deconvoluting this data, demonstrating that there are two clearly separable excitation (solid curves) and emission (dashed curves) bands. We ensured that these spectral components did not change their shape or relative intensities through subsequent rounds of purification; indeed, the di-PDI of interest is present in our samples with high purity (see the Supporting Information). Thus, these two absorption and emission features are intrinsic to the di-PDI molecule.

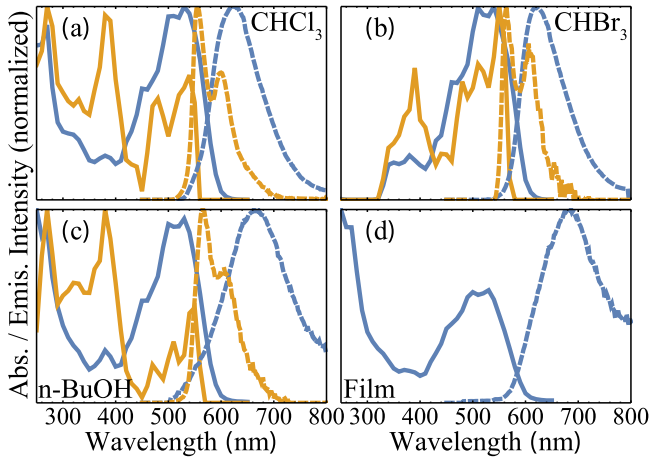

Figure 3. Normalized room-temperature emission spectra (dashed curves) and reconstructed absorption spectra (solid curves) of di-PDI in (a) chloroform, (b) bromoform, (c) 1-butanol, and (d) a pure film; the full 2-D excitation–emission spectra from which these data were constructed are given in the Supporting Information. The red-shifted, broad featureless emission (blue dashed curves) is the major emission contributor, while the narrower, blue-shifted component with a vibronic character has a much smaller contribution (orange dashed curves). The jagged character seen in the reconstructed absorption spectra results from the fact that the raw excitation–emission spectra were taken with 10 nm steps for excitation.

Figure 3a–c shows that in all the solutions that we studied, di-PDI has a broad, red-shifted emission band with a correspondingly broad excitation spectrum (blue curves), as well as a second distinct feature that is only slightly red-shifted and has narrower absorption and emission, both with a pronounced vibronic structure (orange curves). The presence of two distinct absorption and emission components were unexpected, and are further analyzed below. We note that previous experiments on this same di-PDI showed similar emission features, but offered no explanation or assignment.[47] We reconstructed the absorption profiles by taking the independent emission components in linear combination and fitting the total emission profile with a weighted sum of the two emission components at each excitation wavelength. The weightings thus map out an effective absorption spectrum at the resolution of our excitation–emission spectroscopy excitation step size, which was 10 nm; details of our reconstruction procedure are given in the Supporting Information. The fits show that the relative amounts of each underlying component are not equal: the broad absorption/emission component is clearly dominant, capturing the vast majority (>90%) of the overall room-temperature absorption and emission profiles.

The two di-PDI emission profiles in Figure 3 are normalized, but they have very different fluorescence quantum yields. We were able to determine the quantum yield for the broad feature, which can be excited cleanly to the red of 550 nm, by comparison with a fluorescein standard in slightly basic ethanol. Then, using the known yield for the broad feature, we were also able to extract the relative emission yield of the

DOI: 10.1021/acs.jpcc.8b11493
J. Phys. Chem. C 2019, 123, 2127–2138

narrow feature. The yields for the two di-PDI emission components in each of the solvents that we studied in Figure 3 are given in Table 1. The general trend is that the narrow, blue-shifted feature has a quantum yield that is a factor of 2−3 higher than that of the broad, red-shifted feature; neither feature has a quantum yield that approaches that of the PDI monomer, which is essentially unity.[48−50] The quantum yield values we find in chloroform for the broad feature are reasonably similar to those found previously in toluene by Horinouchi et al.[47] The quantum yield we observe in bromoform appears to be higher than that in the other solvents, as discussed in the Supporting Information. We also note that when di-PDI is spin-cast into a thin film (Figure 3d), no narrow emission is observed, as discussed further below.

Table 1. Quantum and Relative Yields for Broad & Narrow Emission Features

solvent	ε	η (mPa s)	Φ_{broad}	Φ_{narrow}
$CHCl_3$	4.8	0.5	0.15 ± 0.1	0.47 ± 0.3
$CHBr_3$	4.3	1.9	0.23 ± 0.15	0.21 ± 0.14
1-BuOH	17.8	2.6	0.05 ± 0.03	0.49 ± 0.4

Although the origin of the narrow and broad spectral components remains to be understood, it is tempting to borrow the standard language of intermolecular aggregation and phenomenologically label the broad red-shifted component as "H-like" and the narrower blue-shifted feature as "J-like".[19] We will argue below, however, that the intramolecular coupling in this molecule is such that these labels do not really apply. Instead, we will posit that the two components result from two distinct molecular conformations: an "open" conformation with the two monomer subunits oriented at near right angles, leading to the broad emission, and a "closed" conformation in which the two monomer subunits are strongly π-stacked.

Temperature Dependence and Population Ratios of the Narrow- and Broad-Emitting Species. With the above experiments pointing to the possibility of two independent spectroscopic species for the di-PDI molecule, we turn now to decoupling their relative absorption cross sections and population ratios. In particular, in this section, we ask what role temperature plays in the existence of these two species and any interconversion process that might connect them. Thus, we conducted fluorescence experiments as a function of temperature in 2-methyl-tetrahydrofuran (2-Me-THF) and 1,2-dichlorobenzene (ODCB), the results of which are shown in Figure 4. Panel (a) shows normalized emission spectra, which indicate that thermal motions play an important role as far as the breadth of the emission is concerned: at liquid N_2 temperatures (black curve), we see complete removal of the narrow, blue-shifted emission band. Moreover, the full width at half-maximum of the broad di-PDI emission component that remains loses ∼30 meV of broadening relative to that at room temperature emission (red curve). This strong temperature dependence to the inhomogeneous broadening may play a significant role in temperature-dependent carrier mobility of di-PDI films, where the barrier for charge transport by hopping is dependent on the distribution of thermally populated states. The narrowing of the broad emission feature and loss of the blue-shifted emission band are entirely reversible when the sample recovers to room temperature. This observation thus indicates that the broad and narrow features thermally interconvert, and that the narrow feature has a higher-energy ground state than that of the broad component, consistent with the idea that they could be two conformations of the same molecule.

Figure 4b shows the relative intensities of the broad di-PDI emission in 2-Me-THF at 150 and 77 K: the emission quantum

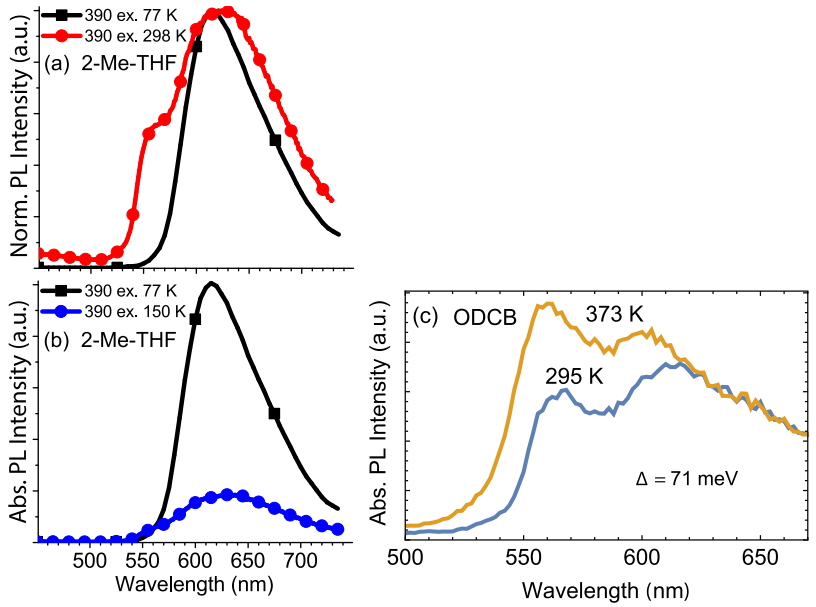

Figure 4. (a) Normalized emission of di-PDI in 2-Me-THF collected at 77 K (black squares) and room temperature (red circles). (b) Absolute emission intensity of di-PDI in 2-Me-THF collected at 77 K (black squares) and 150 K (blue circles). At 77 K, the emission both narrows and increases by a factor of six in intensity. (c) Absolute fluorescence intensity of di-PDI in ODCB at 295 K (blue) and at 373 K (orange). Based on Boltzmann statistics, the change in relative intensity or the narrow emission between 295 and 373 K results in an energy gap of ∼71 meV or just under $3k_BT$ at room temperature.

DOI: 10.1021/acs.jpcc.8b11493
J. Phys. Chem. C 2019, 123, 2127−2138

yield increases by a factor of ~6 at the lower temperature. If we assume that this increase by a factor of six brings the quantum yield of the broad emission band to near unity, then this puts an upper limit on the room-temperature quantum yield of 1.0/6 = 0.17. This upper limit estimate is in excellent quantitative agreement with the measured room-temperature quantum yield of the broad emission between 0.1 and 0.2 in Table 1. Although the quantum yield of the di-PDI emission in 2-Me-THF was not previously investigated, our values of 0.1−0.2 for the broad emission agree with those obtained in other solvents.[47] All of these observations provide clear evidence that large-scale thermal motions of the di-PDI molecule, likely involving ϕ, are critical for nonradiative coupling between the ground and excited states.

Next, we turn to calculating the relative population ratios of the two di-PDI emitting species and the relative energy gap between the ground states of the broad and narrow spectral features. At 77 K, there is simply too little of the narrow spectral feature to reliably measure. Thus, we turn to higher temperatures in order to obtain a quantitative population ratio of the broad and narrow spectral components. We achieved this by studying di-PDI in ODCB at both 295 and 373 K, as shown in Figure 4c. Indeed, consistent with the cryogenic experiments discussed above, we see that as the temperature is raised, there is an increase in the population leading to the narrow emission feature relative to that of the broad feature. On the basis of the measured relative emission intensities and assuming Boltzmann statistics, we calculate that the energy gap between the conformations responsible for the broad and narrow emissions is ~71 meV, or just under $3k_BT$ at room temperature. This is in good agreement with results of our TD-DFT calculations, discussed below, and is also consistent with the cryogenic experiments, where we would predict that the population of the narrow-emitting feature to be negligibly small at 77 K.

We note that the relative energies/populations of the two di-PDI emitting species appear to be solvent dependent. For example, we see less of the narrow feature in chloroform (one of the most widely used solvents for PDIs) than in bromoform (Figure 3) or ODCB. Unfortunately, because of chloroform's low boiling point, we cannot heat the solution to determine the relative stabilities of the two emitting species. As discussed in the Supporting Information, we estimated the energy difference for the narrow- and broad-emitting species in chloroform as ~$5k_BT$ at room temperature based on an argument of conserved oscillator strengths. The fact that the narrow-emitting species is apparently less stable in chloroform may help to explain why it has gone unnoticed until now.

Finally, we note that for di-PDI cast into thin films (Figure 3d), no narrow emission is observed. This is consistent with the idea that excitation of the species that yields the narrow emission feature has a higher-lying lowest unoccupied molecular orbital, so that energy transfer can take place to the larger population of neighboring di-PDI molecules having configurations that produce the broad emission. As discussed further below, our time-resolved anisotropy measurements show little anisotropy in films, even at early times. Thus, although we cannot conclusively prove that energy transfer takes place, the fact that energetic site disorder is well known to lead to energy transfer in films of organic molecules strongly suggests that energy transfer accounts for the absence of the narrow emission in films.[51,52]

TD-DFT Reveals the Broad- and Narrow-Emitting Di-PDI Features to be "Closed" and "Open" Molecular Conformers. To gain additional insight into the assignment of the narrow and broad emission components, we investigated the ground- and excited-state electronic structure of di-PDI via TD-DFT using the methodology described above and in the Supporting Information. Figure 5a shows the calculated

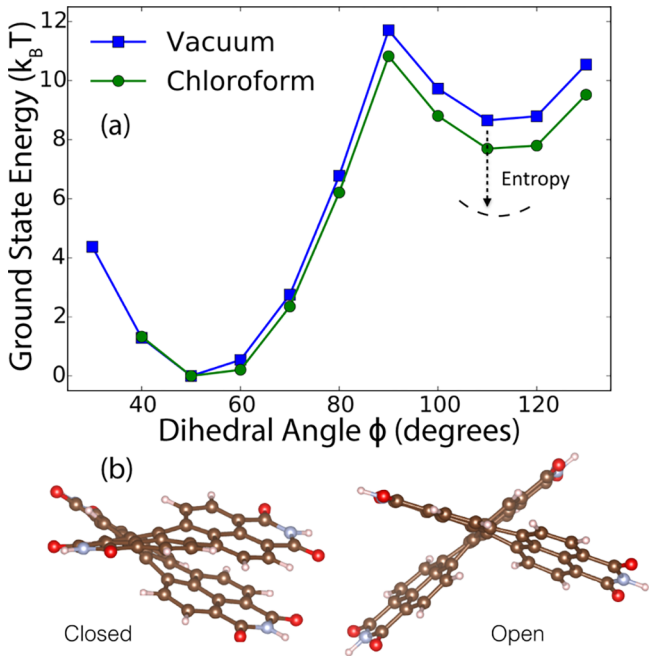

Figure 5. (a) Ground-state potential energy surface of di-PDI computed at the PBE0+D3/6-31++G* level of theory in vacuum (blue squares) and in a polarizable continuum with a dielectric constant of 4.81 (green circles) along the ϕ coordinate (see Figure 1); the zero of energy was chosen to be the global minimum, and the energy scale is in k_BT at room temperature. In addition to the global minimum found at 50°, there is a clear local minimum at 110°. The "closed" structure at 50° has strong π-stacking interactions between the two monomer subunits, as shown at left in panel (b). The more "open" structure with the 110° conformation has the two subunits lying nearly at right angles, as shown at right in panel (b). When entropy effects (calculated from frequency analysis) are included, the relative stability of the open geometry is increased, as indicated by the dashed black curve in (a).

ground-state potential energy surface of di-PDI along the ϕ coordinate in vacuum (blue squares) and in a PCM dielectric of 4.81, chosen to approximate the solution environment of chloroform (green circles). It is worth noting that our definition of the ϕ coordinate is inverted with respect to that of previous studies.[11,23,47] The results in Figure 5a show clearly that there are two distinct energy minima for di-PDI, in accordance with the two observed distinct spectroscopic species observed experimentally. On the basis of their molecular geometries, shown in Figure 5b, we will refer to these two energetic minima as "closed" (for ϕ = 50°) and "open" (for ϕ = 110°). We also note that previous studies have not observed the global minimum for the closed conformer that we see at 50° (or 130° using the definition of previous studies);[11,23,38−42] we believe that this is the result of the fact that previous studies did not employ dispersion correction, which is necessary for describing the π-stacking interactions present between the two molecular subunits when ϕ < 90°.

DOI: 10.1021/acs.jpcc.8b11493
J. Phys. Chem. C 2019, 123, 2127−2138

With the DFT ground-state potential energy surface in hand, we now assign the broad di-PDI emission feature as arising from molecules that have the "closed" geometry. These molecules should predominate in terms of population, have larger coupling between the subunits because of stronger π-interactions (more "H-like"), and given the breadth of the potential surface in ϕ, also show significant inhomogeneous broadening. Conversely, we assign the narrow emission feature to di-PDI molecules with the "open" geometry, which have a smaller population, less coupling between subunits (more "J-like" or monomer-like) and less inhomogeneous broadening. Indeed, the calculated energy difference between the di-PDI "open" and "closed" geometries is $\sim 6k_BT$ in vacuum and $\sim 5k_BT$ in chloroform when entropy effects from frequency analysis are included. These theoretical estimates match well with the population differences that we measured via the temperature-dependent fluorescence experiments, described above.

Figure 6a shows the TD-DFT-calculated energy gaps between the ground state and the first four excited states of di-PDI as a function of ϕ. Panel (b) of this figure shows the ground and first several excited states at the "closed" and "open" geometries; the thickness of the vertical lines represent the oscillator strengths of the transitions between the different states. Clearly, there are many states with transitions contributing to the visible absorption spectrum of the di-PDI molecule, rather than the two states that would be expected from modest coupling between isolated monomer subunits.

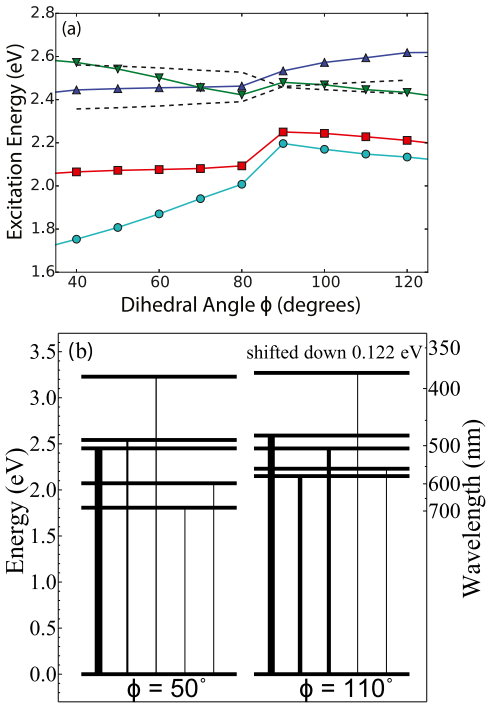

Figure 6. (a) Calculated TD-DFT photoexcitation energies for the first (teal circles), second (red squares), third (green inverted triangles), and fourth (blue upright triangles) excited states of di-PDI as a function of ϕ. The black dashed curves are the estimated Coulombic couplings for two independent monomers calculated from transition point charges. (b) TD-DFT-based energy level diagram for the two di-PDI ground-state minima including the first five excited states; the widths and color saturation of the vertical lines correspond to the oscillator strengths for transitions to each excited state from the ground state. The full ϕ dependence of the oscillator strengths to each of the lowest excited states is available in the Supporting Information.

The dashed curves in panel (a) show the magnitude and sign of what would be expected from Coulombic coupling between independent PDI monomers (with optimized dimer atomic positions and atom-centered monomeric Mulliken transition charges; see the Supporting Information for details). As expected, simple Coulombic coupling changes sign at 90° (the expected switch from H-like to J-like aggregation), and although this somewhat mimics the behavior of the higher-energy transitions, the idea of simple coupling clearly does not work for the di-PDI molecule. Instead, some other form(s) of coupling are more dominant, and/or the molecule cannot be considered as two weakly coupled monomer subunits because of the conjugated bay-linked bridge that connects them. Indeed, because of the bridge, the two monomer subunits are actually radicals rather than closed-shell PDI monomers, and it is the mixing of these states with radical character that we believe leads to the complexity observed in the electronic structure of di-PDI, as discussed further below.

Despite the fact that the electronic structure of di-PDI cannot be explained by simple Davydov splitting, Figure 6 shows that of the lowest four excitations, the upper two transitions carry most of the oscillator strength for the "closed" configuration, while the lower states play a similar role for the "open" geometry. Thus, considered collectively, we see that the "closed" state is somewhat H-like in character, while the "open" geometry can be loosely considered to be J-like. This rough observation is consistent with all of the experiments described above: the "closed" geometry has redder absorption and emission spectra, a weak emission quantum yield, and a greater degree of inhomogeneous broadening, and the "open" geometry has higher oscillator strength to the lowest excited state and thus should exhibit higher fluorescent quantum yields as well as blue-shifted absorption and emission spectra.

In order to better understand how the electronic structure of di-PDI arises, Figure 7 compares the TD-DFT calculated one-electron orbitals for an isolated PDI radical monomer (i.e., half of di-PDI with the connecting bond broken and one electron

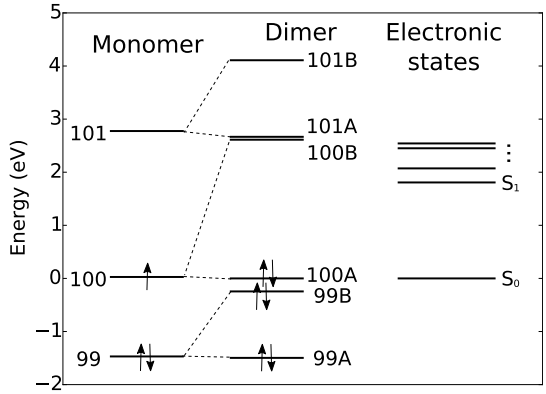

Figure 7. TD-DFT-determined MO electronic energy levels of radical monomer PDI (i.e., half of the di-PDI molecule cleaved along the bay-linked bond), di-PDI one-electron MOs, and the full multiconfigurational di-PDI electronic states, all plotted on the same energy axis. The monomer has an unpaired electron because the dimer is covalently bonded and splitting the bond would result in a radical forming on each half. Note that the MOs of the radical monomers combine to give MOs of di-PDI with different symmetries (labeled A and B).

DOI: 10.1021/acs.jpcc.8b11493
J. Phys. Chem. C 2019, 123, 2127−2138

assigned to each monomer), the di-PDI one-electron MOs, and the full multiconfigurational electronic energy levels of di-PDI. The figure shows a rough match between the energies of a radical monomer and the split dimer one-electron orbitals, further solidifying the idea that di-PDI's electronic structure cannot be explained as an excimer or as two moderately interacting closed-shell monomers. Thus, by linking the PDI monomers through the bay position, the di-PDI molecule behaves more like two mixed/coupled radicals rather than like two separate closed-shell molecules being held in proximity.

Femtosecond Spectroscopy as a Tool to Understand Di-PDI Spectra and Dynamics. With the basic picture of the di-PDI molecule existing in two distinct conformations with different spectral properties strongly supported by both steady-state spectroscopy and TD-DFT calculations, we turn next to femtosecond spectroscopy to understand the conformational dynamics of this molecule. If our picture is correct, then it should be possible to spectrally isolate the "closed" and "open" di-PDI conformers by selective excitation, allowing for independent characterization and the observation of any differences in solvation dynamics or motion along the ϕ coordinate. We also performed an identical set of ultrafast spectroscopy experiments on the PDI monomer, which are detailed in the Supporting Information for comparison. The data shown in the main text were taken with the pump and probe polarizations at the magic angle; polarization-dependent transient absorption is shown in the Supporting Information.

Deconvolving the Absorption Spectra of the Two Di-PDI Conformers with Femtosecond Transient Absorption. Figure 8 shows the results of transient absorption experiments performed with the best excitation wavelengths for isolating the "closed" di-PDI geometry [580 nm, panel (a)] and the "open" di-PDI geometry [400 nm, panel (b)]. For both excitation wavelengths, the negative change in absorption seen to the blue of ∼550 nm consists of a combination of ground-state bleach (GSB)/spectral hole-burning and stimulated emission (SE). The positive ΔOD seen to the red of ∼650 nm is due excited-state absorption (ESA), and the region between 550 and 650 nm contains overlapping ESA and SE signals.

The fact that the shape of the GSB is different for the two excitation wavelengths provides conformation that the steady-state di-PDI absorption spectrum is indeed an inhomogeneous superposition of two different conformers, each of which can be separately excited. The lack of observed spectral diffusion (i.e., the fact that the GSB spectral profiles do not appreciably change other than in overall intensity) from 20 ps to 2 ns also indicates that the two di-PDI conformers do not interchange during the excited-state lifetime: excitation at neither wavelength ultimately leads to the bleaching of the entire steady-state absorption spectrum. This observation fits with our TD-DFT calculations, discussed in the Supporting Information, which shows that the force along the ϕ coordinate following Franck−Condon excitation of both conformers points away from the crossing region, thus effectively inhibiting excited-state interconversion. Therefore, our ultrafast studies are entirely consistent with di-PDI existing as a superposition of two effectively different molecules.

Given the steady-state absorption spectrum, the reconstructed narrow absorption spectrum of the "open" conformer from fluorescence excitation spectroscopy, and the transient GSB spectra from following both 580 and 400 nm excitation, we now have sufficient information from each of these

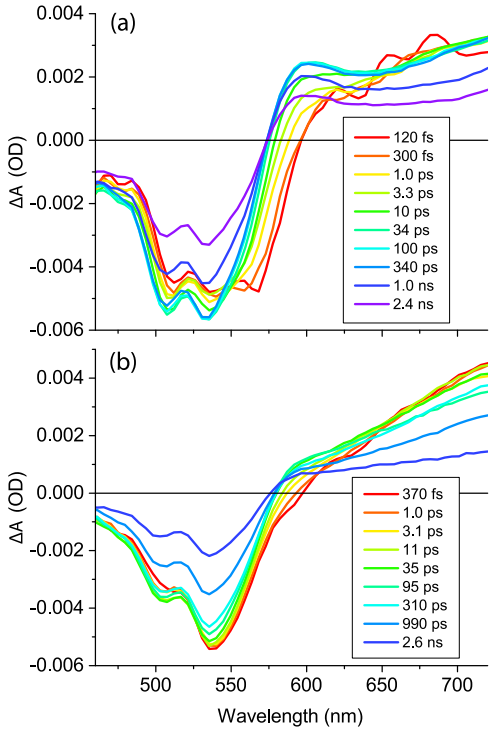

Figure 8. Time-resolved broadband transient absorption of di-PDI in chloroform with 580 nm (upper) and 400 nm (lower) excitation. Spectra are shown in logarithmically spaced time intervals increasing from red to violet. The fact that the transient spectra at the two excitation wavelengths are so different is the direct result of the fact that di-PDI consists of an inhomogeneous superposition of two different conformers.

independent pieces of data to extract the underlying electronic transitions for each di-PDI geometry. We used the standard Gaussian vibronic progression model (described in eq S1 and the accompanying discussion in the Supporting Information). The results of our global fitting procedure are shown in Figure 9, where the data in all four panels (blue circles) were simultaneously fit with the same underlying transitions having fixed amplitude ratios within the separate "closed" and "open" geometries. Three separate transitions were required to fit the spectral profiles at each geometry, leading to six total vibronic progressions. Panels (a) (the steady-state absorption) and (d) (the GSB with 400 nm excitation) contain information about both di-PDI conformations, while panels (b) (the GSB with 580 nm excitation) and (c) (the reconstructed absorption spectrum leading to the narrow emission) contain information primarily about the individual "closed" and "open" geometries, respectively. We constrained the fit to use a single vibronic spacing parameter for each of the three electronic transitions belonging to the "open" and "closed" geometries. Clearly, the results of the fit (solid black curves) are excellent.[47]

When examining the individual electronic transitions comprising the global fit in Figure 9, we see that the "closed" di-PDI geometry electronic transitions are all phenomenologically H-like (with less oscillator strength in the 0−0 transition), while the narrow emission "open" di-PDI geometry transitions appear to have more monomer-like vibronic progressions. This result is qualitatively consistent with the TD-DFT calculations discussed above. It is worth noting that the best fit to the di-PDI absorption spectrum from Horinouchi et al. is similar, but the additional information in

DOI: 10.1021/acs.jpcc.8b11493
J. Phys. Chem. C 2019, 123, 2127−2138

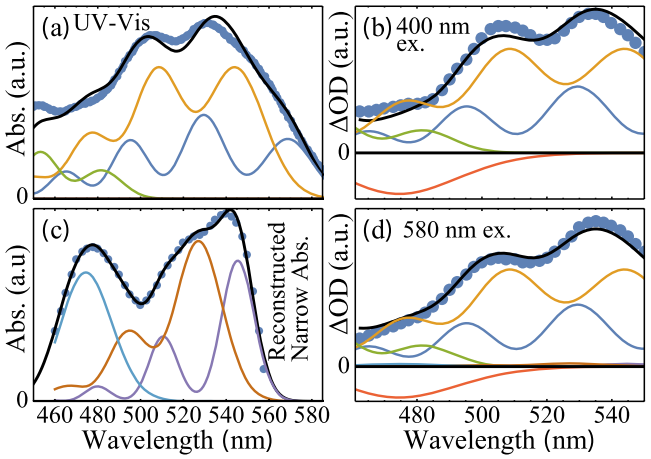

Figure 9. Global fit (black curves) to data from independent spectroscopy experiments (blue circles) performed on di-PDI: (a) steady-state absorption spectrum, (b) ultrafast GSB following 580 nm excitation, (c) reconstructed absorption profile leading to the narrow-band "open" emission, and (d) ultrafast GSB following 400 nm excitation. In panels (b,d), the bleach data are multiplied by −1 for ease of comparison to the absorption spectra, and the horizontal black line marks the zero of transient absorption. The various colored curves show the Gaussian vibronic progressions used to globally fit the data (see the Supporting Information for details). A Gaussian ESA component, required to fit the two transient absorption GSB profiles, is shown as the negative red curve in panels (b,d).

our global fit here constrains the fit better over a wider wavelength range. We also repeated the global fit for di-PDI in other solvents (as detailed in the Supporting Information); the only major difference between solvents is in the relative oscillator strength of the highest energy transition, shown in light blue in panel (c), which decreases with increasing solvent dielectric constant.

Femtosecond Dynamics and Excited-State Lifetimes of the Di-PDI Conformers. Having established that di-PDI is in fact a mixture of "closed" and "open" conformers, in this section, we focus on the early-time dynamics of the molecule following excitation. We began characterizing the observed dynamics by fitting the transient spectroscopy to multi-exponential decays, with no kinetic model implied. The results of this time-domain fitting procedure (see the Supporting Information for details) for both 580 and 400 nm excitation are given in Table 2, which makes clear that di-PDI dynamics take place on a variety of time scales. For both conformers, we observe a small-amplitude fast (<500 fs) component. The amplitude of this component, which is likely due to inertial solvation dynamics, is small enough that it makes little difference in any of the subsequent analysis.

Table 2 and Figure 8 also show that following excitation, di-PDI undergoes a large-amplitude ≤12 ps (in $CHCl_3$) spectral shift that is evident on both edges of the GSB and in the peak position of the ESA. The observed time scale of this shift scales linearly with solvent viscosity, and thus it makes sense to assign this time scale to large-amplitude torsional motion along the ϕ coordinate. This diffusive motion along the internal rotation coordinate is, within error, indistinguishable between the two excitation wavelengths: both "open" and "closed" geometries relax on a similar time scale. This makes sense given that twisting of a monomeric PDI subunit needs to push roughly the same amount of solvent out of the way no matter what the initial geometry.

Table 2. Fitting Parameters to the Dynamics of the Transient Absorption Spectroscopy on Di-PDI (Figure 8) at Two Excitation Wavelengths (580 and 400 nm) and in Several Solvent Environments (See the Supporting Information for Relative Amplitudes of Exponential Components)[a]

environment	τ_1 (ns)	τ_{shift} (ps)	τ_{fast} (ps)
$CHCl_{3,580ex}$	3.9 ± 0.1	12 ± 2	0.3 ± 0.1
$CHBr_{3,580ex}$	3.3 ± 0.7	40 ± 10	0.35 ± 0.2
$1\text{-}BuOH_{580ex}$	1.3 ± 0.4	60 ± 20	<0.15
$Film_{580ex}$	1.8 ± 0.6	60 ± 40	0.3 ± 0.1
$CHCl_{3,400ex}$	3.2 ± 0.4	13 ± 8	
$CHBr_{3,400ex}$	2.8 ± 0.8	45 ± 20	
$1\text{-}BuOH_{400ex}$	1.5 ± 0.2	80 ± 30	<0.2

[a]The results with 580 nm excitation in chloroform agree within error to the measured Kerr-gated fluorescence spectroscopy in Figure 10.

Though their lifetimes are similar, it can be observed that even at ∼2.5 ns, the profiles of the TA spectra with different excitation wavelengths are still distinct. This precludes the existence of significant interconversion between the "open" and "closed" geometries on either the ground or excited states during this period. Furthermore, revisiting the steady-state emission experiments in the context of having two geometries of the same molecule, we also see no cross-emission after preferentially exciting each conformer, even though the temperature-dependent experiment clearly shows they are capable of interconverting on macroscopic time scales.

To better understand the early-time dynamics of di-PDI along the ϕ coordinate, we also measured the time-resolved fluorescence from di-PDI employing Kerr-gated detection at several excitation wavelengths, with the data for 580 nm ("closed") excitation in $CHCl_3$ shown in Figure 10. The time-

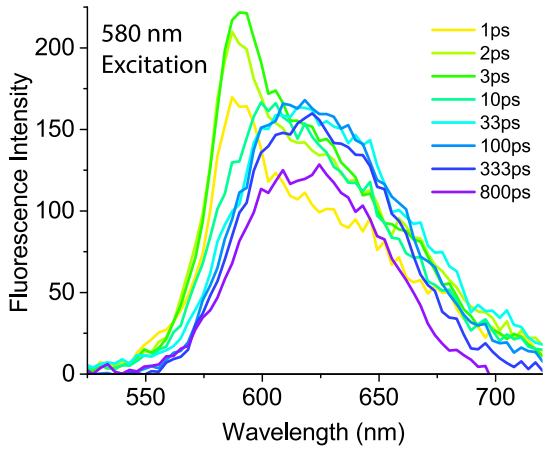

Figure 10. Time-resolved fluorescence from di-PDI in chloroform excited at 580 nm. The data were collected via femtosecond Kerr-gating with carbon disulfide with an effective ∼2 ps time resolution.

resolved Stokes shift shows the same ∼12 ps shift observed in transient absorption, and the overall fluorescence lifetime matches within the error that is found by recovery of the GSB. Also of interest is a sharp emission feature near 590 nm that exists for <10 ps following excitation. This feature does not change as the pump wavelength is tuned between 540 and 580 nm, and is also manifested in the transient absorption data in Figure 8 as an SE (negative) signal peaking near 575 nm for

DOI: 10.1021/acs.jpcc.8b11493
J. Phys. Chem. C 2019, 123, 2127−2138

the first few picoseconds, so we are confident that it is not due to scattering of the pump wavelength. We believe that this short-lived narrow feature results from emission from the Franck−Condon region prior to equilibration along the ϕ coordinate.

The longest time scale reported in Table 2 is the excited-state lifetime of di-PDI, which is on the order of 2−4 ns depending on solvent environment. The lifetimes of two conformers are similar, although it appears that the "open" geometry may have a somewhat shorter lifetime than that of the "closed" geometry (see the Supporting Information for a more detailed analysis). We also see that the total lifetime for both conformers scales inversely with the solvent dielectric constant. Given that the room temperature quantum yield is only 10−20%, this dielectric constant dependence suggests that there may be some slight charge-transfer character to the coordinate that nonadiabatically couples the electronic excited and ground states of both conformers.

Finally, we performed a detailed study of di-PDI orientational dynamics through femtosecond pump-probe polarized anisotropy experiments for the "open" and "closed" geometries; the results are shown in Figure S32 of the Supporting Information, and the measured anisotropy decay times are presented in Table 3. Interestingly, di-PDI shows very little anisotropy, even at the earliest times (∼100 fs). This is a direct result of the fact that both di-PDI conformers have multiple overlapping electronic states, which our TD-DFT calculations suggest are orthogonally polarized (see the Supporting Information for details). This makes it difficult to extract information from our time-resolved anisotropy data (other than the rotational diffusion times shown in Table 3 and the fact that what little anisotropy there is decays much more quickly in films). These experiments bolster the concept of multiple states within each conformation, as shown by the separate global fitting procedure and TD-DFT.

Table 3. Rotational Diffusion Time of Di-PDI in Different Solutions Measured via the Decay of Transient Polarization Anisotropy[a]

environment	$\tau_{r,580}$ (ns)	$\tau_{r,400}$ (ns)
$CHCl_3$	0.5 ± 0.2	0.35 ± 0.3
$CHBr_3$	2.0 ± 0.5	2.1 ± 0.4
1-BuOH	2.2 ± 0.6	2.2 ± 0.7

[a]For reference, the PDI monomer in chloroform exhibits a rotational diffusion time of ∼200 ps.

Photophysical Picture of Di-PDI as Two Molecules in One. Overall, our results from steady-state spectroscopy, TD-DFT calculations, transient absorption, and Kerr-gated fluorescence measurements allow us to propose a complete photophysical picture for di-PDI in solution. Clearly, the molecule exists in two conformations along the dihedral ϕ coordinate. The global minimum "closed" geometry is energetically preferred and accounts for over 90% of di-PDI molecules in solution at room temperature. This conformer is somewhat H-like in its electronic character, with a broad and highly Stokes-shifted emission and an excited-state lifetime of 3.9 ns. The "open" geometry is somewhat harder to characterize given that it comprises <10% of the di-PDI population at room temperature, but it has more J-like character with narrower absorption and emission with little Stokes shift, as well as a somewhat shorter excited-state lifetime.

Following excitation, we see that the GSB, ESA, and luminescence undergo spectral shifts on a viscosity-dependent time scale, which takes ∼12 ps in chloroform. This single time scale appears to describe equilibration on both the ground- and excited-state surfaces for both di-PDI conformers, making it natural to assign this to motion along the important large-amplitude di-PDI degree of freedom: ϕ. Our TD-DFT calculations indicate that the relaxed excited-state geometries are farther from the barrier than the ground-state geometry, especially for the "closed" conformer, as seen in Figure 6. Thus, excitation leads to excited-state twisting along ϕ, and spectral hole-burning along ϕ shows a similar recovery time scale on the ground state (Figure 11).

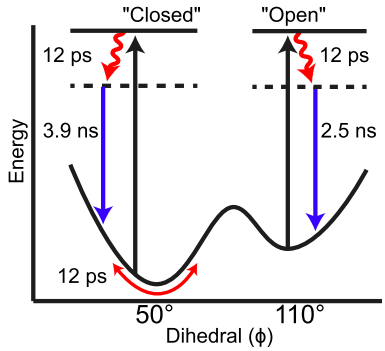

Figure 11. Schematic showing dynamics following photoexcitation of di-PDI. Following excitation and a fast (<300 fs) relaxation to the lowest excited state, both the "open" and "closed" conformers undergo a ∼12 ps (viscosity-dependent) relaxation on their ground and electronic excited states. After the dynamics along ϕ are complete, the two conformers recover to their ground states on a similar ns time scale.

With our combination of different spectroscopies and quantum chemistry calculations, we see that each of the two di-PDI conformations has three (or potentially more) underlying electronic transitions spanning the visible, and that the two conformers are spectrally unique, behaving as distinct molecules that do not interconvert on the time scale of their excited-state lifetimes. Moreover, although these two conformers show some phenomenological similarities to the typical manifestations of H and J intermolecular aggregates, their intramolecular coupling cannot be neglected, requiring a more detailed molecular orbital picture to understand their electronic structure, such as that shown in Figure 7 above.

CONCLUSIONS

In summary, we have investigated the properties of β-β-*S*-di-PDI using a host of steady-state and time-resolved spectroscopies, and have found that there are two distinct conformations of di-PDI at room temperature. The dominant of these conformers has strong π-stacking interactions and is more planar, leading to strong through-space and through-bond intramolecular coupling with phenomenologically H-like spectral properties. The other conformer, previously thought to be dominant from quantum chemistry methods that did not include dispersion, has less intramolecular coupling and appears to have more a more monomer-like or phenomenologically J-like spectrum. Despite the H-like and J-like labels, however, there are multiple electronic transitions for each

DOI: 10.1021/acs.jpcc.8b11493
J. Phys. Chem. C 2019, 123, 2127−2138

conformer that result from direct coupling through the bridging bond and the radical character of the monomer subunits, so that simple aggregation language is not appropriate for describing either form of this molecule. Furthermore, the standard labels of charge-transfer and excimeric states also break down in this limit of direct conjugation.

Our temperature-dependent studies, along with the TD-DFT calculations, allowed us to determine that there is an energy difference of 71 meV, or $\leq 3k_BT$ at room temperature, between the two di-PDI ground-state conformers; indeed, we can "freeze out" the higher-energy "open" conformation by cooling the di-PDI solution to 77 K. The combination of our steady-state and time-resolved spectroscopies allowed us to perform a global fit of the spectra of the two conformers and deconvolve their multiple underlying electronic transitions.

The presence of two conformers has important implications for the use of this class of molecules in optoelectronic devices. The presence of a second conformer in low concentration could act as an exciton or electron trap, possibly diminishing the performance of solar cells or other devices incorporating di-PDIs. On the other hand, if one could engineer the relative distribution of the two conformers, it might be possible to increase light absorption or emission for photovoltaic or organic light-emitting diode applications. Overall, the most important conclusion is that di-PDIs are really two molecules in one, and that di-PDIs need to be treated accordingly if they are to be exploited in working devices.

■ ASSOCIATED CONTENT

Supporting Information

The Supporting Information is available free of charge on the ACS Publications website at DOI: 10.1021/acs.jpcc.8b11493.

Further details of TD-DFT simulations, raw experimental data, and additional details and discussion about the steady-state and time-resolved fitting procedures and outcomes (PDF)

■ AUTHOR INFORMATION

Corresponding Author

*E-mail: schwartz@chem.ucla.edu.

ORCID

Erik P. Farr: 0000-0003-0029-2755

Yves Rubin: 0000-0003-0187-9689

Benjamin J. Schwartz: 0000-0003-3257-9152

Notes

The authors declare no competing financial interest.

■ ACKNOWLEDGMENTS

This work was supported by the National Science Foundation under grant CHE-1565434.

■ REFERENCES

(1) Zhang, G.; Zhao, J.; Chow, P. C. Y.; Jiang, K.; Zhang, J.; Zhu, Z.; Zhang, J.; Huang, F.; Yan, H. Nonfullerene Acceptor Molecules for Bulk Heterojunction Organic Solar Cells. *Chem. Rev.* **2018**, *118*, 3447−3507.

(2) Yan, C.; Barlow, S.; Wang, Z.; Yan, H.; Jen, A. K.-Y.; Marder, S. R.; Zhan, X. Non-Fullerene Acceptors for Organic Solar Cells. *Nat. Rev. Mater.* **2018**, *3*, 18003.

(3) Austin, A.; Hestand, N. J.; McKendry, I. G.; Zhong, C.; Zhu, X.; Zdilla, M. J.; Spano, F. C.; Szarko, J. M. Enhanced Davydov Splitting in Crystals of a Perylene Diimide Derivative. *J. Phys. Chem. Lett.* **2017**, *8*, 1118−1123.

(4) Hestand, N. J.; Spano, F. C. Molecular Aggregate Photophysics beyond the Kasha Model: Novel Design Principles for Organic Materials. *Acc. Chem. Res.* **2017**, *50*, 341−350.

(5) Céspedes-Guirao, F. J.; García-Santamaría, S.; Fernández-Lázaro, F.; Sastre-Santos, A.; Bolink, H. J. Efficient Electroluminescence from a Perylenediimide Fluorophore Obtained from a Simple Solution Processed OLED. *J. Phys. D: Appl. Phys.* **2009**, *42*, 105106.

(6) Kozma, E.; Mróz, W.; Villafiorita-Monteleone, F.; Galeotti, F.; Andicsová-Eckstein, A.; Catellani, M.; Botta, C. Perylene Diimide Derivatives as Red and Deep Red-Emitters for Fully Solution Processable OLEDs. *RSC Adv.* **2016**, *6*, 61175−61179.

(7) Jiang, W.; Ye, L.; Li, X.; Xiao, C.; Tan, F.; Zhao, W.; Hou, J.; Wang, Z. Bay-Linked Perylene Bisimides as Promising Non-Fullerene Acceptors for Organic Solar Cells. *Chem. Commun.* **2014**, *50*, 1024−1026.

(8) Zang, Y.; Li, C.-Z.; Chueh, C.-C.; Williams, S. T.; Jiang, W.; Wang, Z.-H.; Yu, J.-S.; Jen, A. K.-Y. Integrated Molecular, Interfacial, and Device Engineering Towards High-Performance Non-Fullerene Based Organic Solar Cells. *Adv. Mater.* **2014**, *26*, 5708−5714.

(9) Wu, C.-H.; Chueh, C.-C.; Xi, Y.-Y.; Zhong, H.-L.; Gao, G.-P.; Wang, Z.-H.; Pozzo, L. D.; Wen, T.-C.; Jen, A. K.-Y. Influence of Molecular Geometry of Perylene Diimide Dimers and Polymers on Bulk Heterojunction Morphology Toward High-Performance Non-fullerene Polymer Solar Cells. *Adv. Funct. Mater.* **2015**, *25*, 5326−5332.

(10) Zhao, J.; Li, Y.; Lin, H.; Liu, Y.; Jiang, K.; Mu, C.; Ma, T.; Lai, J. Y. L.; Hu, H.; Yu, D.; Yan, H. High-Efficiency Non-Fullerene Organic Solar Cells Enabled by a Difluorobenzothiadiazole-Based Donor Polymer Combined with a Properly Matched Small Molecule Acceptor. *Energy Environ. Sci.* **2015**, *8*, 520−525.

(11) Sun, D.; Meng, D.; Cai, Y.; Fan, B.; Li, Y.; Jiang, W.; Huo, L.; Sun, Y.; Wang, Z. Non-Fullerene-Acceptor-Based Bulk-Heterojunction Organic Solar Cells with Efficiency Over 7%. *J. Am. Chem. Soc.* **2015**, *137*, 11156−11162.

(12) Meng, D.; Sun, D.; Zhong, C.; Liu, T.; Fan, B.; Huo, L.; Li, Y.; Jiang, W.; Choi, H.; Kim, T.; Kim, J. Y.; Sun, Y.; Wang, Z.; Heeger, A. J. High-Performance Solution-Processed Non-Fullerene Organic Solar Cells Based on Selenophene-Containing Perylene Bisimide Acceptor. *J. Am. Chem. Soc.* **2015**, *138*, 375−380.

(13) Lim, J. M.; Kim, P.; Yoon, M.-C.; Sung, J.; Dehm, V.; Chen, Z.; Würthner, F.; Kim, D. Exciton Delocalization and Dynamics in Helical π-stacks of Self-Assembled Perylene Bisimides. *Chem. Sci.* **2013**, *4*, 388−397.

(14) Huang, C.; Barlow, S.; Marder, S. R. Perylene-3,4,9,10-Tetracarboxylic Acid Diimides: Synthesis, Physical Properties, and Use in Organic Electronics. *J. Org. Chem.* **2011**, *76*, 2386−2407.

(15) Fan, Y.; Ziabrev, K.; Zhang, S.; Lin, B.; Barlow, S.; Marder, S. R. Comparison of the Optical and Electrochemical Properties of Bi(perylene diimide)s Linked through Ortho and Bay Positions. *ACS Omega* **2017**, *2*, 377−385.

(16) Langhals, H.; Krotz, O.; Polborn, K.; Mayer, P. A Novel Fluorescent Dye with Strong, Anisotropic Solid-State Fluorescence, Small Stokes Shift, and High Photostability. *Angew. Chem., Int. Ed.* **2005**, *44*, 2427−2428.

(17) Gregg, B. A.; Sprague, J.; Peterson, M. W. Long-Range Singlet Energy Transfer in Perylene Bis(phenethylimide) Films. *J. Phys. Chem. B* **1997**, *101*, 5362−5369.

(18) Qu, J.; Zhang, J.; Grimsdale, A. C.; Müllen, K.; Jaiser, F.; Yang, X.; Neher, D. Dendronized Perylene Diimide Emitters: Synthesis, Luminescence, and Electron and Energy Transfer Studies. *Macromolecules* **2004**, *37*, 8297−8306.

(19) Spano, F. C. The Spectral Signatures of Frenkel Polarons in H- and J-Aggregates. *Acc. Chem. Res.* **2010**, *43*, 429−439.

(20) Son, M.; Park, K. H.; Shao, C.; Würthner, F.; Kim, D. Spectroscopic Demonstration of Exciton Dynamics and Excimer Formation in a Sterically Controlled Perylene Bisimide Dimer Aggregate. *J. Phys. Chem. Lett.* **2014**, *5*, 3601−3607.

DOI: 10.1021/acs.jpcc.8b11493
J. Phys. Chem. C 2019, 123, 2127−2138

(21) Son, M.; Park, K. H.; Yoon, M.-C.; Kim, P.; Kim, D. Excited-State Vibrational Coherence in Perylene Bisimide Probed by Femtosecond Broadband Pump-Probe Spectroscopy. *J. Phys. Chem. A* **2015**, *119*, 6275−6282.
(22) Sung, J.; Nowak-Król, A.; Schlosser, F.; Fimmel, B.; Kim, W.; Kim, D.; Würthner, F. Direct Observation of Excimer-Mediated Intramolecular Electron Transfer in a Cofacially-Stacked Perylene Bisimide Pair. *J. Am. Chem. Soc.* **2016**, *138*, 9029−9032.
(23) Jiang, W.; Xiao, C.; Hao, L.; Wang, Z.; Ceymann, H.; Lambert, C.; Di Motta, S.; Negri, F. Localization/Delocalization of Charges in Bay-Linked Perylene Bisimides. *Chem.—Eur. J.* **2012**, *18*, 6764−6775.
(24) Yan, Q.; Zhou, Y.; Zheng, Y.-Q.; Pei, J.; Zhao, D. Towards Rational Design of Organic Electron Acceptors for Photovoltaics: A Study Based on Perylenediimide Derivatives. *Chem. Sci.* **2013**, *4*, 4389−4394.
(25) Herrmann, A.; Weil, T.; Sinigersky, V.; Wiesler, U.-M.; Vosch, T.; Hofkens, J.; De Schryver, F. C.; Müllen, K. Polyphenylene Dendrimers with Perylene Diimide as a Luminescent Core. *Chem.—Eur. J.* **2001**, *7*, 4844−4853.
(26) Hochstrasser, R. M.; Kasha, M. Application of the Exciton Model To Mono-Molecular Lamellar Systems. *Photochem. Photobiol.* **1964**, *3*, 317−331.
(27) Kasha, M.; Rawls, H. R.; El-Bayoumi, M. A. The Exciton Model in Molecular Spectroscopy. *Pure Appl. Chem.* **1965**, *11*, 371−392.
(28) Gao, F.; Zhao, Y.; Liang, W. Vibronic Spectra of Perylene Bisimide Oligomers: Effects of Intermolecular Charge-Transfer Excitation and Conformational Flexibility. *J. Phys. Chem. B* **2011**, *115*, 2699−2708.
(29) Spreitler, F.; Sommer, M.; Hollfelder, M.; Thelakkat, M.; Gekle, S.; Köhler, J. Unravelling the Conformations of Di-(Perylene Bisimide Acrylate) by Combining Time-Resolved Fluorescence-Anisotropy Experiments and Molecular Modelling. *Phys. Chem. Chem. Phys.* **2014**, *16*, 25959−25968.
(30) Würthner, F.; Saha-Möller, C. R.; Fimmel, B.; Ogi, S.; Leowanawat, P.; Schmidt, D. Perylene Bisimide Dye Assemblies as Archetype Functional Supramolecular Materials. *Chem. Rev.* **2015**, *116*, 962−1052.
(31) Giaimo, J. M.; Lockard, J. V.; Sinks, L. E.; Scott, A. M.; Wilson, T. M.; Wasielewski, M. R. Excited Singlet States of Covalently Bound, Cofacial Dimers and Trimers of Perylene-3,4:9,10-bis-(dicarboximide)s. *J. Phys. Chem. A* **2008**, *112*, 2322−2330.
(32) Veldman, D.; Chopin, S. M. A.; Meskers, S. C. J.; Groeneveld, M. M.; Williams, R. M.; Janssen, R. A. J. Triplet Formation Involving a Polar Transition State in a Well-Defined Intramolecular Perylenediimide Dimeric Aggregate. *J. Phys. Chem. A* **2008**, *112*, 5846−5857.
(33) Zhang, J.; Li, Y.; Huang, J.; Hu, H.; Zhang, G.; Ma, T.; Chow, P. C. Y.; Ade, H.; Pan, D.; Yan, H. Ring-Fusion of Perylene Diimide Acceptor Enabling Efficient Nonfullerene Organic Solar Cells with a Small Voltage Loss. *J. Am. Chem. Soc.* **2017**, *139*, 16092−16095.
(34) Frisch, M. J.; Trucks, G. W.; Schlegel, H. B.; Scuseria, G. E.; Robb, M. A.; Cheeseman, J. R.; Scalmani, G.; Barone, V.; Petersson, G. A.; Nakatsuji, H. *Gaussian 16*, Revision A.03; Gaussian Inc.: Wallingford CT, 2016.
(35) Krylov, A. I.; Gill, P. M. W. Q-Chem: An Engine for Innovation. *Wiley Interdiscip. Rev.: Comput. Mol. Sci.* **2012**, *3*, 317−326.
(36) Adamo, C.; Barone, V. Toward Reliable Density Functional Methods Without Adjustable Parameters: The PBE0 Model. *J. Chem. Phys.* **1999**, *110*, 6158−6170.
(37) Grimme, S.; Antony, J.; Ehrlich, S.; Krieg, H. A Consistent and Accurate ab initio Parametrization of Density Functional Dispersion Correction (DFT-D) for the 94 elements H-Pu. *J. Chem. Phys.* **2010**, *132*, 154104.
(38) Zhan, C.; Yao, J. More than Conformational "Twisting" or "Coplanarity": Molecular Strategies for Designing High-Efficiency Nonfullerene Organic Solar Cells. *Chem. Mater.* **2016**, *28*, 1948−1964.
(39) Hwang, S.; Potscavage, W. J.; Nakamichi, R.; Adachi, C. Processing and Doping of Thick Polymer Active Layers for Flexible Organic Thermoelectric Modules. *Org. Electron.* **2016**, *31*, 31−40.
(40) Hartnett, P. E.; Matte, H. S. S. R.; Eastham, N. D.; Jackson, N. E.; Wu, Y.; Chen, L. X.; Ratner, M. A.; Chang, R. P. H.; Hersam, M. C.; Wasielewski, M. R.; Marks, T. J. Ring-Fusion as a Perylenediimide Dimer Design Concept for High-Performance Non-Fullerene Organic Photovoltaic Acceptors. *Chem. Sci.* **2016**, *7*, 3543−3555.
(41) Wang, B.; Liu, W.; Li, H.; Mai, J.; Liu, S.; Lu, X.; Li, H.; Shi, M.; Li, C.-Z.; Chen, H. Electron Acceptors with Varied Linkages Between Perylene Diimide and Benzotrithiophene for Efficient Fullerene-Free Solar Cells. *J. Mater. Chem. A* **2017**, *5*, 9396−9401.
(42) Cann, J.; Dayneko, S.; Sun, J.-P.; Hendsbee, A. D.; Hill, I. G.; Welch, G. C. N-Annulated Perylene Diimide Dimers: Acetylene Linkers as a Strategy for Controlling Structural Conformation and the Impact on Physical, Electronic, Optical and Photovoltaic Properties. *J. Mater. Chem. C* **2017**, *5*, 2074−2083.
(43) Barone, V.; Cossi, M. Quantum Calculation of Molecular Energies and Energy Gradients in Solution by a Conductor Solvent Model. *J. Phys. Chem. A* **1998**, *102*, 1995−2001.
(44) Mulliken, R. S. Electronic Population Analysis on LCAO-MO Molecular Wave Functions. I. *J. Chem. Phys.* **1955**, *23*, 1833−1840.
(45) Farr, E. P.; Zho, C.-C.; Challa, J. R.; Schwartz, B. J. Temperature Dependence of the Hydrated Electron's Excited-State Relaxation. II. Elucidating the Relaxation Mechanism Through Ultrafast Transient Absorption and Stimulated Emission spectroscopy. *J. Chem. Phys.* **2017**, *147*, 074504.
(46) Oliver, T. A. A.; Zhang, Y.; Roy, A.; Ashfold, M. N. R.; Bradforth, S. E. Exploring Autoionization and Photoinduced Proton-Coupled Electron Transfer Pathways of Phenol in Aqueous Solution. *J. Phys. Chem. Lett.* **2015**, *6*, 4159−4164.
(47) Horinouchi, H.; Sakai, H.; Araki, Y.; Sakanoue, T.; Takenobu, T.; Wada, T.; Tkachenko, N. V.; Hasobe, T. Controllable Electronic Structures and Photoinduced Processes of Bay-Linked Perylenediimide Dimers and a Ferrocene-Linked Triad. *Chem.—Eur. J.* **2016**, *22*, 9631−9641.
(48) Ford, W. E.; Kamat, P. V. Photochemistry of 3,4,9,10-Perylenetetracarboxylic Dianhydride Dyes. 3. Singlet and Triplet Excited-State Properties of the bis(2,5-di-tert-butylphenyl)imide Derivative. *J. Phys. Chem.* **1987**, *91*, 6373−6380.
(49) Gvishi, R.; Reisfeld, R.; Burshtein, Z. Spectroscopy and Laser Action of the "Red Perylimide Dye" in Various Solvents. *Chem. Phys. Lett.* **1993**, *213*, 338−344.
(50) Supur, M.; El-Khouly, M. E.; Seok, J. H.; Kim, J. H.; Kay, K.-Y.; Fukuzumi, S. Efficient Electron Transfer Processes of the Covalently Linked Perylenediimide- Ferrocene Systems: Femtosecond and Nanosecond Transient Absorption Studies. *J. Phys. Chem. C* **2010**, *114*, 10969−10977.
(51) Deledalle, F.; Tuladhar, P. S.; Nelson, J.; Durrant, J. R.; Kirchartz, T. Understanding the Apparent Charge Density Dependence of Mobility and Lifetime in Organic Bulk Heterojunction Solar Cells. *J. Phys. Chem. C* **2014**, *118*, 8837−8842.
(52) Finck, B. Y.; Schwartz, B. J. Drift-Diffusion Studies of Compositional Morphology in Bulk Heterojunctions: The Role of the Mixed Phase in Photovoltaic Performance. *Phys. Rev. Appl.* **2016**, *6*, 054008.

DOI: 10.1021/acs.jpcc.8b11493
J. Phys. Chem. C 2019, 123, 2127−2138